
Extracting Training Data from Unconditional Diffusion Models

Yunhao Chen
Fudan University
dongdongunique@gmail.com

Xingjun Ma
Fudan University
xingjunma@fudan.edu.cn

Difan Zou
University of Hong Kong
dzou@cs.hku.hk

Yu-Gang Jiang
Fudan University
ygj@fudan.edu.cn

Abstract

As diffusion probabilistic models (DPMs) are being employed as mainstream models for generative artificial intelligence (AI), the study of their memorization of the raw training data has attracted growing attention. Existing works in this direction aim to establish an understanding of whether or to what extent DPMs learn by memorization. Such an understanding is crucial for identifying potential risks of data leakage and copyright infringement in diffusion models and, more importantly, for more controllable generation and trustworthy application of Artificial Intelligence Generated Content (AIGC). While previous works have made important observations of when DPMs are prone to memorization, these findings are mostly empirical, and the developed data extraction methods only work for conditional diffusion models. In this work, we aim to establish a theoretical understanding of memorization in DPMs with 1) a memorization metric for theoretical analysis, 2) an analysis of conditional memorization with informative and random labels, and 3) two better evaluation metrics for measuring memorization. Based on the theoretical analysis, we further propose a novel data extraction method called **Surrogate conditional Data Extraction (SIDE)** that leverages a classifier trained on generated data as a surrogate condition to extract training data directly from unconditional diffusion models. Our empirical results demonstrate that SIDE can extract training data from diffusion models where previous methods fail, and it is on average over 50% more effective across different scales of the CelebA dataset.

1 Introduction

The diffusion probabilistic models (DPMs) [11, 20, 24] is one family of powerful generative models that learn the distribution of a dataset by first gradually destroying the structure of the data through an iterative forward diffusion process and then restoring the data structure via a reverse diffusion process. Due to their outstanding capability in capturing data distribution, DPMs have become the foundation models for many pioneering generative artificial intelligence (AI) products such as Stable Diffusion [18], DALL-E 3 [1], and Sora [2]. Despite the widespread adoption of DPMs, a potential risk they face is *data memorization*, i.e., the risk of memorizing a certain proportion of the raw training samples. This could result in the generation of memorized (rather than new) samples via direct copying, which could cause data leakage, privacy breaches, or copyright infringement, as highlighted in the literature [21, 22]. Furthermore, data memorization also gives rise to data extraction attacks which is a type of privacy attacks that attempt to extract the raw training data from a well-trained model. Notably, a recent work by Carlini et al. [4] demonstrated the feasibility of extracting training data samples from DPMs like Stable Diffusion [18], revealing the potential dangers associated with these models.



Figure 1: A few examples of the extracted images from a DDPM trained on a subset of the CelebA dataset using our SIDE method. *Top*: training images; *bottom*: extracted images.

While several works have investigated the data memorization phenomenon in diffusion models, the results are mostly empirical. For example, it has been observed that there exists a strong correlation between training data memorization and conditional DPMs [22, 8], i.e., conditional DPMs can memorize more raw training samples. Although these observations have deepened our understanding of diffusion models, a theoretical characterization of the underlying memorization mechanism of DPMs is still missing in the current literature. In this paper, we propose a theoretical framework to explain the mechanisms underpinning training data memorization in DPMs. A recent study conducted by Gu et al. [8] reveals that utilizing randomly initialized class labels for conditional training dramatically increases data memorization in diffusion models. We extend this finding by providing a theoretical explanation for why it leads to increased memorization.

Meanwhile, the work by Somepalli et al. [22] highlights a key distinction between conditional and unconditional DPMs, i.e., data replication is more common in the former but uncommon in the latter. While this understanding is important, existing data extraction methods can only extract training data from conditional DPMs. Arguably, unconditional DPMs are the base foundation of real-world applications, posing a practical challenge for data extraction. For example, Stable Diffusion is composed of an unconditional diffusion model and a text-image guidance. In this work, we aim to establish a theoretical understanding that can help us achieve scalable data extraction directly from unconditional DPMs. To this end, we propose a novel data extraction method called **Surrogate conditional Data Extraction (SIDE)** to extract training data from unconditional diffusion models. We hope this development can further highlight the potential risks associated with DPMs.

In summary, our main contributions are:

- We propose a theoretical framework that explains the underlying mechanism of data memorization in conditional generative models, which advances our understanding beyond empirical observations. Moreover, this framework also explains the increased data memorization when randomly initialized class labels are used during conditional training.
- We introduce a novel data extraction attack called *Surrogate conditional Data Extraction (SIDE)* that can extract training data from unconditional diffusion models, a challenging task where all previous methods could fail. SIDE is 50% more effective on average over all the evaluation metrics across different sizes of the CelebA dataset.
- We propose two new metrics including the average memorization score (AMS) and unique memorization score (UMS) to measure the memorization effect from two different angles. These two metrics are validated based on both theoretical and empirical analyses.

2 Related Work

Diffusion Probabilistic Models (DPMs) DPMs [20] (or diffusion models) have largely replaced GANs. They achieve state-of-the-art performance on academic benchmarks [7] and underpin popular image generators like Stable Diffusion [18], DALL-E 3 [1], Sora [2], Runway [18], and Imagen [19]. These models can be viewed from two perspectives. The first is score matching [24], where diffusion models learn the gradient of the image distribution [25]. The second perspective involves denoising DPMs [11], which add Gaussian noise at various time steps to clean images and train models to

denoise them. To conditionally sample from diffusion models, [7] utilizes a classifier to guide the denoising process at each sampling step, aligning with our data extraction method. Additionally, [12] introduces classifier-free guidance for conditional data sampling using DPMs.

Memorization in Diffusion Models Recent investigations into DPMs have shed light on their data memorization behaviors. Somepalli et al. [21] found that 0.5-2% of images generated by these models are object-level duplicates of the training samples, a finding corroborated by Carlini et al. [4] which uses the text-conditional diffusion models to extract memorized dataset. Somepalli et al. [22] and Gu et al. [8] delved into the causative factors behind such memorization phenomena and found that being conditioned plays a crucial role in memorization and unconditional models are less prone to memorization. However, existing understandings of data memorization in generative models have largely been empirical, as evidenced by research focused on generative language models [3, 13] or diffusion models [22, 8]. In this work, we aim to provide a theoretical explanation for memorization in conditional diffusion models which further motivates a novel data extraction method for unconditional diffusion models.

3 Proposed Theory and Method

In this section, we introduce a theoretical memorization metric and provide a theoretical explanation for the universality of data memorization in conditional diffusion models. Based on our theoretical explanation, we further propose a novel data extraction method for unconditional diffusion models.

3.1 Memorization Metric

Intuitively, the memorization of fixed training data points (i.e., point-wise memorization) can be quantified by the degree of overlap between the generated distribution and the distributions centered at each data point. Given a generative model f_θ with parameters θ and training dataset $\mathcal{D} = \{\mathbf{x}_i\}_{i=1}^N$, we propose the following *memorization metric* to quantify the degree of memorization in f_θ about the training data samples:

$$\mathcal{M}(\mathcal{D}; \theta) = \sum_{\mathbf{x}_i \in \mathcal{D}} \int p_\theta(\mathbf{x}) \log \frac{p_\theta(\mathbf{x})}{q(\mathbf{x}, \mathbf{x}_i, \epsilon)} d\mathbf{x}, \quad (1)$$

where $\mathbf{x}_i \in \mathbb{R}^d$ is the i -th training sample, N is the total number of training samples, $p_\theta(\mathbf{x})$ represents the probability density function (PDF) of the generated samples, and $q(\mathbf{x}, \mathbf{x}_i, \epsilon)$ is the probability distribution characterizing training data point \mathbf{x}_i . Note that $q(\mathbf{x}, \mathbf{x}_i, \epsilon)$ may not be a true data distribution, for example, $q(\mathbf{x}, \mathbf{x}_i, \epsilon)$ could be a Dirac delta function centered at training data point \mathbf{x}_i : $q(\mathbf{x}, \mathbf{x}_i, \epsilon) = \delta(\mathbf{x} - \mathbf{x}_i)$. However, we do not use the Dirac delta function for $q(\mathbf{x}, \mathbf{x}_i, \epsilon)$ because it is not computable within the Kullback–Leibler (KL) divergence framework. Alternatively, we use the Gaussian distribution with a covariance matrix ϵI (I is the identity matrix and $0 < \epsilon < 1$ is a scalar with a small positive value) to define $q(\mathbf{x}, \mathbf{x}_i, \epsilon)$ as:

$$q(\mathbf{x}, \mathbf{x}_i, \epsilon) = \frac{1}{\sqrt{(2\pi\epsilon)^d}} \exp \left\{ -\frac{1}{2\epsilon} (\mathbf{x} - \mathbf{x}_i)^\top (\mathbf{x} - \mathbf{x}_i) \right\}. \quad (2)$$

Note that in Equation (1), a smaller value of $\mathcal{M}(\mathcal{D}; \theta)$ close to zero indicates more memorization.

3.2 Conditional Memorization

Informative Labels Our theoretical understanding is developed based on the concept of *informative labels*. While informative labels have been discussed in previous works [8] as class labels, here we define a generalized version of it that takes class labels and random labels as its special cases. Let $\mathcal{Y} = \{y_1, y_2, \dots, y_C\}$ be the label set for training dataset \mathcal{D} with C unique labels. Here, the labels are not limited to the conventional class labels, they can also be text captions, shared features, or cluster information that can be used to group the training samples into subsets. Let y_i be the associated label with \mathbf{x}_i , and $\mathcal{D}_{y=c} = \{\mathbf{x}_i : \mathbf{x}_i \in \mathcal{D}, y_i = c\}$ is the subset of training samples shared the same label $y = c$. We define an informative label as follows:

Definition 1 (Informative Label) A label $y = c$ is said to be an informative label if it satisfies $|\mathcal{D}_{y=c}| < |\mathcal{D}|$.

The above definition states that an information label should have the ability to differentiate a subset of samples from others. An extreme case is that all samples have the same label, and in this case, the label is not an informative label. Note that, according to our definition, both class labels and random labels are special cases of information labels. Informative labels can be either *explicit* like the paired class/random labels and text captions, or *implicit* like silent features or deep representation clusters. Next, we will define the correlation between informative labels and the clustering effect in the representation space of a generative model that has an encoder and decoder. For example, the encoder of diffusion models is the forward diffusion process (adding noise), and the decoder of it is the reverse diffusion process (denoising).

Suppose we have an encoder $f_{\theta_E}(\mathbf{x})$ and a decoder $f_{\theta_D}(\mathbf{z})$. The encoder $f_{\theta_E}(\mathbf{x})$ maps data samples $\mathbf{x} \in \mathcal{D}$ to the latent distribution \mathbf{z} which is assumed to follow a normal distribution $\mathcal{N}(\boldsymbol{\mu}, \boldsymbol{\Sigma})$: $p_{\theta}(\mathbf{z}) = \mathcal{N}(\boldsymbol{\mu}, \boldsymbol{\Sigma})$. For $\mathbf{x}_i \in \mathcal{D}_{y=c}$, the encoder maps \mathbf{x}_i to a latent distribution \mathbf{z}_c subject to $\mathcal{N}(\boldsymbol{\mu}_c, \boldsymbol{\Sigma}_c)$, i.e., $p_{\theta}(\mathbf{z}|y=c) = \mathcal{N}(\boldsymbol{\mu}_c, \boldsymbol{\Sigma}_c)$. The decoder $f_{\theta_D}(\mathbf{z})$ maps \mathbf{z} back to the original data samples \mathbf{x} . y_i is the label of data sample \mathbf{x}_i . Training a generative f_{θ} is to optimize the following likelihood estimation:

$$\min - \sum_{\mathbf{x}_i \in \mathcal{D}} \log p_{\theta}(\mathbf{x}_i | y_i). \quad (3)$$

Proposition 1 *If f_{θ} converges on objective 3, then for the latent space \mathbf{z} conditioned on an informative label $y = c$, we have following two properties under reasonable assumption:*

$$\|\boldsymbol{\Sigma}_c\|_* \leq \|\boldsymbol{\Sigma}\|_* \quad (4)$$

$$\sum_{\mathbf{z}_i \in \mathcal{D}_{y=c}^z} (\mathbf{z}_i - \boldsymbol{\mu}_c)^T (\mathbf{z}_i - \boldsymbol{\mu}_c) \leq \sum_{\mathbf{z}_i \in \mathcal{D}^z} (\mathbf{z}_i - \boldsymbol{\mu})^T (\mathbf{z}_i - \boldsymbol{\mu}). \quad (5)$$

$\|\cdot\|_*$ is the nuclear norm with a smaller value indicating less information due to the sum of the matrix's singular values. In Proposition 1, our assumption is that $p_{\theta}(\mathbf{z}|y)$, being conditional, contains less information than $p_{\theta}(\mathbf{z})$. Consequently, the nuclear norm of the $p_{\theta}(\mathbf{z}|y)$'s covariance matrix is smaller than $p_{\theta}(\mathbf{z})$.

Intuitively, Equation (5) implies that the latent code of each training sample conditioned on an informative label $y = c$ is more centered around the distribution $p_{\theta}(\mathbf{z}|y = c)$ than $p_{\theta}(\mathbf{z})$. Previous work [8] has revealed that the presence of informative labels significantly influences the memorization behavior of conditional generative models. Informative labels provide additional context or specifics about the data, thus aiding the model in learning specific data features more effectively. We formalize this observation through the following theorem:

Theorem 1 *A generative model f_{θ} occurs a higher degree of memorization when conditioned on informative labels y , mathematically expressed as:*

$$\lim_{\epsilon \rightarrow 0} \frac{\sum_{\mathbf{x}_i \in \mathcal{D}_{y=c}} \int p_{\theta}(\mathbf{x}|y=c) \log \frac{p_{\theta}(\mathbf{x}|y=c)}{q(\mathbf{x}, \mathbf{x}_i, \epsilon)} d\mathbf{x}}{\sum_{\mathbf{x}_i \in \mathcal{D}_{y=c}} \int p_{\theta}(\mathbf{x}) \log \frac{p_{\theta}(\mathbf{x})}{q(\mathbf{x}, \mathbf{x}_i, \epsilon)} d\mathbf{x}} \leq 1. \quad (6)$$

The proof is in Appendix A.2. Theorem 1 states that when conditioned on information labels, the generative model would generate a data distribution that has more overlap with the point-wise distributions $q(\mathbf{x}, \mathbf{x}_i, \epsilon)$, leading to more memorization and a lower $\mathcal{M}(\mathcal{D}; \theta)$ (integrated KL divergence) value.

Memorization with Explicit Informative Labels As explained above, informative labels can either be explicit like class labels or implicit like clusters. Previous works revealed that 1) conditional training of diffusion models incurs more memorization [8], and 2) data replications are more common in conditional diffusion models [22]. Following our theoretical framework introduced above, the conditions used in training a conditional diffusion model are often text captions or class concepts, which are all informative labels that satisfy Definition 1. Thus, according to Theorem 1, these informative labels result in more memorization than without them. It has also been discovered in [8] that random labels can also lead to a stronger memorization effect. According to Definition 1, random labels are also information labels, i.e., each label defines a unique subset of the training samples. In this case, the model will be forced to overfit the training samples conditioned on randomly assigned informative labels.

3.3 Surrogate conditional Data Extraction(SIDE)

Here, we introduce our SIDE method designed for extracting training data from unconditional diffusion models. There exist no explicit information labels in unconditional diffusion models. However, our theoretical analysis implies that informative labels could emerge even when generative models are trained unconditionally. In this case, the informative labels can be implicit labels like cluster centers formed during the training process. Next, we will construct implicit informative labels for unconditional diffusion models, convert the implicit labels into explicit ones, and then leverage the explicit labels to extract training data from unconditional diffusion models.

3.3.1 Constructing Implicit Informative Labels

We could use a classifier that can identify the implicit label y_I in the sampling process of the diffusion model to condition the implicit labels for diffusion models. The classifier can be a normal classifier trained on the same data as the target diffusion model. When such a classifier is not available, our analysis in Section 3.2 indicates that random labels or cluster information extracted by a pre-trained feature extractor (e.g., the CLIP image encoder) can be used as the implicit labels. We assume that there exists an implicit label y_I learned by the unconditional diffusion model. Then, the sampling process for diffusion models can be represented as follows:

$$d\mathbf{x} = [f(\mathbf{x}, t) - g(t)^2 (\nabla_{\mathbf{x}} \log p_{\theta}^t(\mathbf{x}|y_I))] dt + g(t)dw \quad (7)$$

$$d\mathbf{x} = [f(\mathbf{x}, t) - g(t)^2 (\nabla_{\mathbf{x}} \log p_{\theta}^t(\mathbf{x}) + \nabla_{\mathbf{x}} \log p_{\theta}^t(y_I|\mathbf{x}))] dt + g(t)dw, \quad (8)$$

where x represents the state vector, $f(x, t)$ denotes the drift coefficient, $g(t)$ is the diffusion coefficient, $\nabla_{\mathbf{x}} \log p_{\theta}^t(\mathbf{x})$ signifies the gradient of the neural network p_{θ} given \mathbf{x} at time t , the neural network is trained to approximate the true data distribution $p(\mathbf{x})$. dw corresponds to the increment of the Wiener process. $\nabla_{\mathbf{x}} \log p_{\theta}^t(y_I|\mathbf{x})$ represents the gradient of the conditional distribution of y_I given x .

To get the gradient of the implicit labels, we use the classifier that generates the implicit label to approximate the gradient. However, a well-known challenge associated with neural network classifiers is their tendency towards miscalibration, as highlighted by [9]. Specifically, the classifier could be overconfident or underconfident of their output. To mitigate the potential impact of classifier miscalibration on the sampling procedure, we introduce a hyperparameter λ to calibrate the classifier’s probability output on the diffusion path using power prior as follows:

$$p_{\theta}^t(\mathbf{x}|y_I) \propto p_{\theta}^{t\lambda}(y_I|\mathbf{x}) p_{\theta}^t(\mathbf{x}). \quad (9)$$

Then, we have:

$$d\mathbf{x} = [f(\mathbf{x}, t) - g(t)^2 (\nabla_{\mathbf{x}} \log p_{\theta}^t(\mathbf{x}) + \lambda \nabla_{\mathbf{x}} \log p_{\theta}^t(y_I|\mathbf{x}))] dt + g(t)dw. \quad (10)$$

This sampling process was initially proposed in [7] for a different purpose, and our deprivation is different from [7]. It is worth mentioning that, in [7], they assumed that $\int p_{\theta}^{t\lambda}(y|\mathbf{x}) dy = Z$ with Z being a constant. However, this assumption only holds when $\lambda = 1$, as Z is explicitly dependent on the \mathbf{x}_t (the t -th step of sampling image \mathbf{x}) when $\lambda \neq 1$. Our derivation solves this issue by redefining the $q_{\theta}^t(y|\mathbf{x})$ using power prior.

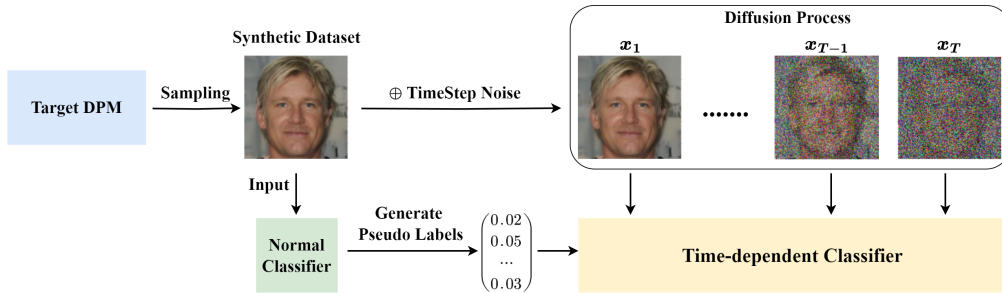


Figure 2: An illustration of our proposed time-dependent knowledge distillation (TDKD) that trains a time-dependent classifier on a pseudo-labeled synthetic dataset.

3.3.2 Time-dependent Classifier

In Equation (10), the classifier is denoted by $\log p_\theta^t(y|\mathbf{x})$, implying its time-dependent nature. However, we do not have a time-dependent classifier at hand but only a time-independent classifier by our assumption. To address this problem, we propose a method named *Time-Dependent Knowledge Distillation* (TDKD) to train a time-dependent classifier. The distillation process is illustrated in Figure 2. TDKD equips classifier models with time-dependent guidance during sampling. It operates in two steps: first, the network architecture is adjusted to accommodate time-dependent inputs; second, a generative dataset and associated labels are created to facilitate knowledge distillation from the normal classifier to its time-dependent counterpart.

Specifically, we incorporate a simple time-dependent module into each basic block to refine the network architecture, with only a minimal modification to the original architecture. The structure of the time-dependent module and modification are illustrated in Appendix C. As the original training dataset is unknown, we employ the target diffusion model to generate a synthetic dataset, following the generative data augmentation techniques [6, 5]. Then, we use the normal classifier trained on the original dataset to generate pseudo labels for the generated images. Finally, we modify the architecture of the normal classifier to add the time-dependent module and train a time-dependent classifier on the labeled synthetic dataset. The objective of this training is to minimize the following loss function:

$$\mathcal{L}_{distil} = D_{KL} (p_\theta(y_I|\mathbf{x}), p_\theta^t(y_I|\mathbf{x}_t)). \quad (11)$$

Overall Pipeline With the trained time-dependent classifier $p_\theta^t(y|\mathbf{x}_t)$ and the target diffusion model, our SIDE extracts training data from the diffusion model following a conditional generation process. Assume we condition on the label $y = c$. Firstly, we choose a set of $\lambda: \mathcal{D}_\lambda$ to conduct the SIDE attack. Secondly, we sample N_G data samples for different λ in the \mathcal{D}_λ . During each sampling timestep t , we compute the gradient $C\nabla_{\mathbf{x}_t} CE(c, p_\theta^t(y|\mathbf{x}_t))$ ($CE(\cdot)$ is the cross-entropy loss), then we use the gradient and the diffusion models to reverse the diffusion process. Thirdly, we compute the similarity score for each generated image. Finally, we evaluate the attack performance using certain evaluation metrics and average the performance of different λ as the final results.

3.4 Performance Metric

Arguably, it is extremely challenging to determine where a generative image is an extract memorization (copy) of a particular training image, as in this case, the L_p distances are no longer meaningful. As such, previous research adopts the Self-Supervised Descriptor for Image Copy Detection (SSCD) score to identify similar image pairs [21, 8]. They calculate the SSCD score between each generated image and each training image to find the most similar training image. Then, they take the mean SSCD score of the top-5% generated images having the highest SSCD scores to measure the extraction performance. This metric has two major issues: 1) it cannot measure uniqueness, i.e., the number of unique images memorized by the model, which we believe is a fundamental measure for memorization; 2) it cannot accurately estimate the total number of memorized samples if cutoff at 95-th percentile (as the model could memorize more than 5% of the training samples).

To address the limitation of the existing measure, here we first categorize the SSCD similarity score into three levels: 1) *low similarity* with SSCD score below 0.5; 2) *mid similarity* with SSCD score between 0.5 and 0.6; and 3) *high similarity* with SSCD scores above 0.6. We then define the following two new performance metrics. The first is the **Average Memorization Score (AMS)**:

$$AMS(\mathcal{D}_{gen}, \mathcal{D}_{train}, \alpha, \beta) = \frac{\sum_{\mathbf{x}_i \in \mathcal{D}_{gen}} \mathcal{F}(\mathbf{x}_i, \mathcal{D}_{train}, \alpha, \beta)}{N_G}. \quad (12)$$

The second is the **Unique Memorization Score (UMS)**:

$$UMS(\mathcal{D}_{gen}, \mathcal{D}_{train}, \alpha, \beta) = \frac{|\bigcup_{\mathbf{x}_i \in \mathcal{D}_{gen}} \phi(\mathbf{x}_i, \mathcal{D}_{train}, \alpha, \beta)|}{N_G}, \quad (13)$$

where N_G is the number of generated images, \mathcal{D}_{gen} is the generated dataset, \mathcal{D}_{train} is the training dataset, and α, β are thresholds for image similarity scoring. $\mathcal{F}(\mathbf{x}_i, \mathcal{D}_{train}, \alpha, \beta)$ returns 1 if the highest SSCD score satisfies the condition between \mathbf{x}_i and \mathcal{D}_{train} ; otherwise, it returns 0. $\phi(\mathbf{x}_i, \mathcal{D}_{train}, \alpha, \beta)$ returns the index of the training dataset image with an SSCD score within the range; if no data satisfy

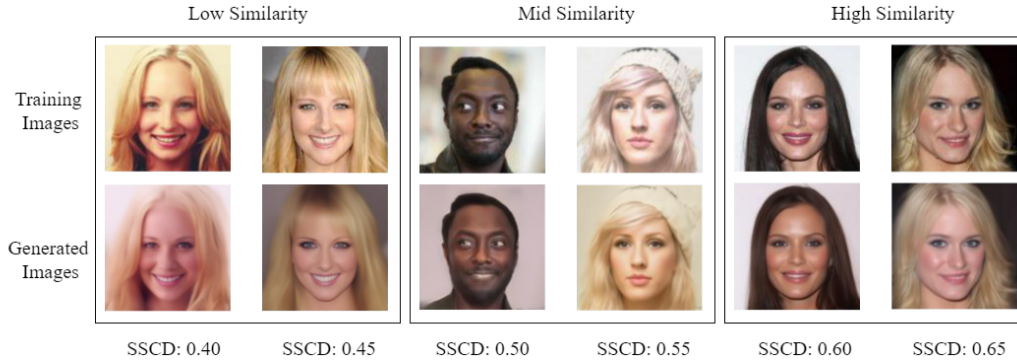


Figure 3: A example comparison between the original training images (top row) and generated images (bottom row) by our SIDE method. The matches are classified into three categories based on their similarity scores: low similarity (SSCD score < 0.5), mid similarity (SSCD score between 0.5 and 0.6), and high similarity (SSCD score > 0.6). This classification demonstrates varying degrees of semantic resemblance and detail replication across the image pairs.

the condition, it returns \emptyset . By considering all near-duplicate images, AMS addresses the first issue of previous evaluation metrics. UMS effectively captures the uniqueness of memorization in data extraction, overcoming the previous metric’s inaccuracy in estimating the uniqueness of memorized samples. In our context, the thresholds for similarity classifications are defined as follows: $\alpha = 0.4$ and $\beta = 0.5$ for low similarity, $\alpha = 0.5$ and $\beta = 0.6$ for middle similarity, and $\alpha = 0.6$ and $\beta = 1.0$ for high similarity.

4 Experiments

In this section, we first introduce our experiment setting including the datasets and models, and then present the main evaluation results of our SIDE method. We also conducted an ablation study replacing the classifier used in SIDE with a few alternatives. Finally, we analyze the sensitive of SIDE to its hyperparameter λ .

4.1 Experimental Setup

We use two datasets to evaluate the effectiveness of our SIDE method: CelebA-HQ-Face-Identity (CelebA-HQ-FI) [16] which consists of 5478 images and a subset of the CelebA (CelebA-25000) [14] which contains 25,000 images. All the images are resized to 128×128 and normalized to $[-1, 1]$. We use the AdamW optimizer[15] with a learning rate of $1e-4$ to train the time-dependent classifier. We train denoising diffusion probabilistic models with a discrete denoising scheduler (DDIM [23]) on the two datasets using the HuggingFace implementation[17]. All diffusion models are trained with a batch size of 64. The diffusion model is trained for 258k (≈ 3000 epochs) steps for the CelebA-HQ-FI dataset and 390k steps (≈ 1000 epochs) for the CelebA-25000 dataset. We use ResNet34[10] as the normal classifier which is further modified to obtain the architecture of time-dependent classifier.

4.2 Main Results

We first evaluate the effectiveness of our SIDE method on CelebA-HQ-F and CelebA-25000 datasets. We compare SIDE with a random baseline (which was also explored in [4]) and its variants constructed by replacing its time-dependent classifier with an alternative classifier. "TD" denotes a time-dependent classifier trained using our proposed TDKD method, "TI" denotes the time-independent classifier, and "OL" denotes training with the dataset’s original labels. The "Random" baseline generates images directly using the target unconditional diffusion model, which is exactly the same method of [4]. We average the results across various λ (defined in Equation (10)) values ranging from 5 to 9, with detailed analysis provided in subsection 4.3. Note that $\lambda = 0$ corresponds to the "Random" baseline. For each λ including $\lambda = 0$, we generate 50,000 images to validate our theoretical analysis and the

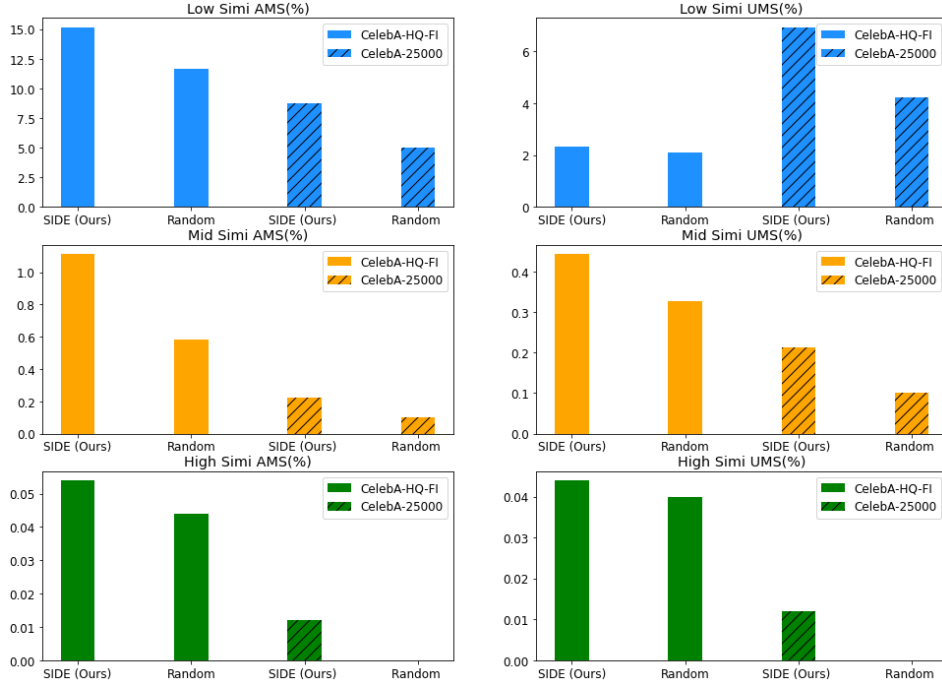


Figure 4: The main results of our SIDE method, ‘Random’ refers to the baseline that generate images directly using the target unconditional diffusion model.

Table 1: The extraction performance of our SIDE method and its variants on CelebA-25000 and CelebA-HQ-FI.

| Dataset | Method | Low Similarity | | Mid Similarity | | High Similarity | |
|--------------|-------------|----------------|--------------|----------------|--------------|-----------------|--------------|
| | | AMS(%) | UMS(%) | AMS(%) | UMS(%) | AMS(%) | UMS(%) |
| CelebA-HQ-FI | Random | 11.656 | 2.120 | 0.596 | 0.328 | 0.044 | 0.040 |
| | OL-TI | 2.649 | 0.744 | 0.075 | 0.057 | 0.005 | 0.005 |
| | SIDE (Ours) | 15.172 | 2.342 | 1.115 | 0.444 | 0.054 | 0.044 |
| CelebA-25000 | Random | 5.000 | 4.240 | 0.100 | 0.100 | 0.000 | 0.000 |
| | OL-TI | 0.164 | 0.152 | 0.000 | 0.000 | 0.000 | 0.000 |
| | SIDE (Ours) | 8.756 | 6.940 | 0.224 | 0.212 | 0.012 | 0.012 |

proposed SIDE method. This crafts one of the largest-scale generated image sets in this field for the memorization study of diffusion models.

Effectiveness of SIDE The AMS and UMS results of our SIDE compared with the ‘Random’ baseline at the low, mid, and high similarity levels are shown in Figure 4. It is evident that our proposed SIDE is highly effective in extracting training data across all three levels of similarity criteria. It remarkably succeeds in extracting memorized (high similarity) training data from the CelebA-25000 dataset, a task previously deemed unfeasible due to the dataset’s scale of over 10,000 samples [21]. The AMS measures the percentage of memorized images, and the UMS measures uniquely memorized images in a generated set. In CelebA-HQ-FI, the SIDE method increases mid-level AMS by $\approx 87\%$ to 1.115%, equating to 111 images per 10,000 being mid-level memorized. It also boosts mid-level UMS by $\approx 37\%$ to 0.444%, meaning 44 images per 10,000 are uniquely memorized. SIDE improves AMS and UMS by $\approx 20\%$ on average for other similarity levels. In the CelebA-25000 dataset, SIDE dramatically enhances AMS and UMS. For low similarity, AMS and UMS increase by 75% and 63%, respectively. For mid similarity, AMS improves by 124% and UMS by 112%. For high similarity, SIDE successfully extracts memorized data, unlike the unconditional model.

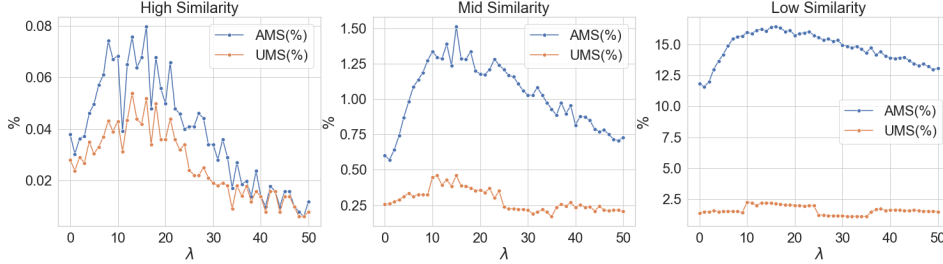


Figure 5: Hyper-parameter (λ) analysis on CelebA-HQ-FI. For high similarity, the best λ for AMS and UMS are 16 and 13. For other similarity levels, the best λ for AMS and UMS is 13.

Effectiveness of TDKD As can be observed in Table 1, classifiers that are independent of time demonstrate significantly inferior performance compared to their time-dependent counterparts. Specifically, their effectiveness is approximately 10% of that observed in classifiers trained to utilize the TDKD method. The underlying reason for this discrepancy is that the classifier is expected to yield accurate gradients at each timestep. However, time-independent classifiers are only capable of providing accurate gradients at the final timestep despite being thoroughly trained. In contrast, the DDPM requires accurate gradients across 1000 timesteps, and the DDIM necessitates accurate gradients for at least 50 timesteps. Consequently, without training that incorporates time dependency, the performance of the classifier significantly deteriorates.

Random Labels We also use random labels to train the classifier with one sample assigned with one unique data label. In CelebA-25000, AMS and UMS for low, middle, and high similarity are 5.448%, 4.620%, 0.176%, 0.164%, 0%, and 0%, respectively. The metrics suffer due to insufficient data samples per class, hindering the classifier’s ability to learn robust representations. With only one sample per class, the classifier struggles to provide accurate gradients, leading to poorer performance in the time-dependent classifier trained based on it.

4.3 Hyper-parameter Analysis

Here, we test the sensitivity of SIDE to its hyper-parameter λ . To this end, we generate 50,000 images for each integer value of λ within the range of $[0, 50]$. As shown in Figure 5, the memorization score increases at first, reaching its highest, then decreases as λ increases. This can be understood from sampling SDE Equation (10). Starting from 0, the diffusion models are unconditional. As λ increases, the diffusion models become conditional, and according to Theorem 1, the memorization effect will be triggered. However, when λ is too large, the generated images will overfit the classifier’s decision boundaries, leading to a low diversity and ignoring the data distribution. Consequently, the memorization score will be decreased.

5 Conclusion

In this paper, we studied the data memorization effect in diffusion models. We introduced a memorization metric to quantify the memorization effect between generated samples and the raw training data points. We then provided a theoretical analysis of the conditional memorization observation in previous works with a generalized definition of informative labels and explained that random labels are also informative. We further differentiate informative labels into *explicit labels* vs. *implicit labels*. Based on such a differentiation, we propose a novel method called *Surrogate conditional Data Extraction (SIDE)* to extract training data from unconditional diffusion models. SIDE constructs a surrogate condition using a classifier trained on the same training dataset as the target diffusion model. We revealed the key to incorporating such a surrogate condition into a training data extraction method is training a time-dependent classifier using the proposed *Time-Dependent Knowledge Distillation (TDKD)* technique. We empirically verify the effectiveness of SIDE on two subsets of the CelebA dataset with two new proposed memorization scores Average Memorization Score (AMS) and Unique Memorization Score (UMS). We hope our work can help understand the memorization mechanism of diffusion models and motivate more advanced data extraction methods.

References

- [1] James Betker et al. “Improving Image Generation with Better Captions”. In: URL: <https://api.semanticscholar.org/CorpusID:264403242>.
- [2] Tim Brooks et al. “Video generation models as world simulators”. In: (2024). URL: <https://openai.com/research/video-generation-models-as-world-simulators>.
- [3] Nicholas Carlini et al. “Quantifying memorization across neural language models”. In: *arXiv preprint arXiv:2202.07646* (2022).
- [4] Nicolas Carlini et al. “Extracting training data from diffusion models”. In: *32nd USENIX Security Symposium (USENIX Security 23)*. 2023, pp. 5253–5270.
- [5] Yunhao Chen, Zihui Yan, and Yunjie Zhu. “A Unified Framework for Generative Data Augmentation: A Comprehensive Survey”. In: *ArXiv abs/2310.00277* (2023). URL: <https://api.semanticscholar.org/CorpusID:263334452>.
- [6] Yunhao Chen et al. “Data Augmentation for Environmental Sound Classification Using Diffusion Probabilistic Model with Top-K Selection Discriminator”. In: *International Conference on Intelligent Computing*. Springer. 2023, pp. 283–295.
- [7] Prafulla Dhariwal and Alexander Nichol. “Diffusion models beat gans on image synthesis”. In: *Advances in neural information processing systems* 34 (2021), pp. 8780–8794.
- [8] Xiangming Gu et al. “On Memorization in Diffusion Models”. In: *ArXiv abs/2310.02664* (2023). URL: <https://api.semanticscholar.org/CorpusID:263620137>.
- [9] Chuan Guo et al. “On calibration of modern neural networks”. In: *International conference on machine learning*. PMLR. 2017, pp. 1321–1330.
- [10] Kaiming He et al. “Deep Residual Learning for Image Recognition”. In: *2016 IEEE Conference on Computer Vision and Pattern Recognition (CVPR)* (2015), pp. 770–778. URL: <https://api.semanticscholar.org/CorpusID:206594692>.
- [11] Jonathan Ho, Ajay Jain, and Pieter Abbeel. “Denosing diffusion probabilistic models”. In: *Advances in neural information processing systems* 33 (2020), pp. 6840–6851.
- [12] Jonathan Ho and Tim Salimans. “Classifier-free diffusion guidance”. In: *arXiv preprint arXiv:2207.12598* (2022).
- [13] Matthew Jagielski et al. “Measuring forgetting of memorized training examples”. In: *arXiv preprint arXiv:2207.00099* (2022).
- [14] Ziwei Liu et al. “Deep Learning Face Attributes in the Wild”. In: *Proceedings of International Conference on Computer Vision (ICCV)*. Dec. 2015.
- [15] Ilya Loshchilov and Frank Hutter. “Decoupled Weight Decay Regularization”. In: *International Conference on Learning Representations*. 2019. URL: <https://openreview.net/forum?id=Bkg6RiCqY7>.
- [16] Dongbin Na, Sangwoo Ji, and Jong Kim. “Unrestricted Black-Box Adversarial Attack Using GAN with Limited Queries”. In: *European Conference on Computer Vision*. Springer. 2022, pp. 467–482.
- [17] Patrick von Platen et al. *Diffusers: State-of-the-art diffusion models*. <https://github.com/huggingface/diffusers>. 2022.
- [18] Robin Rombach et al. “High-resolution image synthesis with latent diffusion models”. In: *Proceedings of the IEEE/CVF conference on computer vision and pattern recognition*. 2022, pp. 10684–10695.
- [19] Chitwan Saharia et al. “Photorealistic text-to-image diffusion models with deep language understanding”. In: *Advances in neural information processing systems* 35 (2022), pp. 36479–36494.
- [20] Jascha Sohl-Dickstein et al. “Deep unsupervised learning using nonequilibrium thermodynamics”. In: *International conference on machine learning*. PMLR. 2015, pp. 2256–2265.
- [21] Gowthami Somepalli et al. “Diffusion Art or Digital Forgery? Investigating Data Replication in Diffusion Models”. In: *2023 IEEE/CVF Conference on Computer Vision and Pattern Recognition (CVPR)* (2022), pp. 6048–6058. URL: <https://api.semanticscholar.org/CorpusID:254366634>.
- [22] Gowthami Somepalli et al. “Understanding and mitigating copying in diffusion models”. In: *Advances in Neural Information Processing Systems* 36 (2023), pp. 47783–47803.

- [23] Jiaming Song, Chenlin Meng, and Stefano Ermon. “Denoising Diffusion Implicit Models”. In: *International Conference on Learning Representations*. 2021. URL: <https://openreview.net/forum?id=St1giarCHLP>.
- [24] Yang Song and Stefano Ermon. “Generative modeling by estimating gradients of the data distribution”. In: *Advances in neural information processing systems* 32 (2019).
- [25] Yang Song et al. “Score-based generative modeling through stochastic differential equations”. In: *arXiv preprint arXiv:2011.13456* (2020).

A

A.1 Preliminaries

If $p(x)$ and $q(x)$ are normal distributions:

$$p(\mathbf{x}) = \frac{1}{\sqrt{(2\pi)^d \det(\boldsymbol{\Sigma}_p)}} \exp \left\{ -\frac{1}{2} (\mathbf{x} - \boldsymbol{\mu}_p)^\top \boldsymbol{\Sigma}_p^{-1} (\mathbf{x} - \boldsymbol{\mu}_p) \right\} \quad (14)$$

$$q(\mathbf{x}) = \frac{1}{\sqrt{(2\pi)^d \det(\boldsymbol{\Sigma}_q)}} \exp \left\{ -\frac{1}{2} (\mathbf{x} - \boldsymbol{\mu}_q)^\top \boldsymbol{\Sigma}_q^{-1} (\mathbf{x} - \boldsymbol{\mu}_q) \right\} \quad (15)$$

Then they have:

$$\mathbb{E}_{\mathbf{x} \sim p(\mathbf{x})} \left[(\mathbf{x} - \boldsymbol{\mu}_q)^\top \boldsymbol{\Sigma}_q^{-1} (\mathbf{x} - \boldsymbol{\mu}_q) \right] \quad (16)$$

$$= \text{Tr}(\boldsymbol{\Sigma}_q^{-1} \boldsymbol{\Sigma}_p) + (\boldsymbol{\mu}_p - \boldsymbol{\mu}_q)^\top \boldsymbol{\Sigma}_q^{-1} (\boldsymbol{\mu}_p - \boldsymbol{\mu}_q) \quad (17)$$

$$(18)$$

$$\mathbb{E}_{\mathbf{x} \sim q(\mathbf{x})} \left[(\mathbf{x} - \boldsymbol{\mu}_q)^\top \boldsymbol{\Sigma}_q^{-1} (\mathbf{x} - \boldsymbol{\mu}_q) \right] = d \quad (19)$$

The entropy of $p(x)$:

$$H_p(\mathbf{x}) = \mathbb{E}_{\mathbf{x} \sim p(\mathbf{x})} [-\log p(\mathbf{x})] = \frac{n}{2} (1 + \log 2\pi) + \frac{1}{2} \log \det(\boldsymbol{\Sigma}_p) \quad (20)$$

The KL divergence between the two distributions is:

$$D_{KL}(p(\mathbf{x}) \| q(\mathbf{x})) \quad (21)$$

$$= \frac{1}{2} \left[(\boldsymbol{\mu}_p - \boldsymbol{\mu}_q)^\top \boldsymbol{\Sigma}_q^{-1} (\boldsymbol{\mu}_p - \boldsymbol{\mu}_q) - \log \det(\boldsymbol{\Sigma}_q^{-1} \boldsymbol{\Sigma}_p) + \text{Tr}(\boldsymbol{\Sigma}_q^{-1} \boldsymbol{\Sigma}_p) - d \right] \quad (22)$$

A.2 Proof for theorem 1

This section will detail the proof for the theorem 1. Assuming we have an encoder $f_{\theta_E}(\mathbf{x})$ and a decoder $f_{\theta_D}(\mathbf{z})$. $f_{\theta_E}(\mathbf{x})$ can map data samples \mathbf{x} to the latent distribution \mathbf{z} , which subjects to a normal distribution $N(\boldsymbol{\mu}, \boldsymbol{\Sigma})$, $\mathbf{z} \in \mathbb{R}^d$. $f_{\theta_D}(\mathbf{z})$ maps the \mathbf{z} to the original data samples.

$$\lim_{\epsilon \rightarrow 0} \frac{\sum_{\mathbf{x}_i \in \mathcal{D}_{y=c}} \int p_\theta(\mathbf{x}|y=c) \log \frac{p_\theta(\mathbf{x}|y=c)}{q(\mathbf{x}, \mathbf{x}_i, \epsilon)} d\mathbf{x}}{\sum_{\mathbf{x}_i \in \mathcal{D}_{y=c}} \int p_\theta(\mathbf{x}) \log \frac{p_\theta(\mathbf{x})}{q(\mathbf{x}, \mathbf{x}_i, \epsilon)} d\mathbf{x}} \leq 1 \quad (23)$$

Also, based on the transformation of PDF and the method of change of variables for multiple integrals, we can have:

$$p_\theta(\mathbf{x}|y=c) = p_\theta(\mathbf{z}|y=c) \det \left(\frac{\partial \mathbf{z}}{\partial \mathbf{x}} \right) = p_\theta(\mathbf{z}|y=c) \det \left(\frac{\partial f_{\theta_E}(\mathbf{x})}{\partial \mathbf{x}} \right) \quad (24)$$

$$p_\theta(\mathbf{x}) = p_\theta(\mathbf{z}) \det \left(\frac{\partial \mathbf{z}}{\partial \mathbf{x}} \right) = p_\theta(\mathbf{z}) \det \left(\frac{\partial f_{\theta_E}(\mathbf{x})}{\partial \mathbf{x}} \right) \quad (25)$$

$$q(\mathbf{x}; \mathbf{x}_i) = q(\mathbf{z}; \mathbf{z}_i) \det \left(\frac{\partial \mathbf{z}}{\partial \mathbf{x}} \right) = q(\mathbf{z}; \mathbf{z}_i) \det \left(\frac{\partial f_{\theta_E}(\mathbf{x})}{\partial \mathbf{x}} \right) \quad (26)$$

$$d\mathbf{x} = \det \left(\frac{\partial \mathbf{x}}{\partial \mathbf{z}} \right) d\mathbf{z} = \det \left(\frac{\partial f_{\theta_D}(\mathbf{z})}{\partial \mathbf{z}} \right) d\mathbf{z} = \det \left(\frac{\partial \mathbf{x}}{\partial f_{\theta_E}(\mathbf{x})} \right) d\mathbf{z} \quad (27)$$

Define $\mathcal{D}_{y=c}^z = \{\mathbf{z}_i : f_{\theta_E}(\mathbf{x}_i) \in \mathcal{D}_{y=c}\}$

$\mathcal{D}_{y=c} = \{\mathbf{x}_i : \mathbf{x}_i \in \mathcal{D}, y_i = c\}$

Then (23) will be:

$$\lim_{\epsilon \rightarrow 0} \frac{\sum_{\mathbf{x}_i \in \mathcal{D}_{y=c}} \int p_\theta(\mathbf{x}|y=c) \log \frac{p_\theta(\mathbf{x}|y=c)}{q(\mathbf{x}, \mathbf{x}_i, \epsilon)} d\mathbf{x}}{\sum_{\mathbf{x}_i \in \mathcal{D}_{y=c}} \int p_\theta(\mathbf{x}) \log \frac{p_\theta(\mathbf{x})}{q(\mathbf{x}, \mathbf{x}_i, \epsilon)} d\mathbf{x}} \leq 1 \quad (28)$$

$$\Rightarrow \lim_{\epsilon \rightarrow 0} \frac{\sum_{\mathbf{z}_i \in \mathcal{D}_{\hat{y}=c}^z} \int p_\theta(\mathbf{z}|y=c) \log \frac{p_\theta(\mathbf{z}|y=c)}{q(\mathbf{z}, \mathbf{z}_i, \epsilon)} d\mathbf{z}}{\sum_{\mathbf{z}_i \in \mathcal{D}_{y=c}^z} \int p_\theta(\mathbf{z}) \log \frac{p_\theta(\mathbf{z})}{q(\mathbf{z}, \mathbf{z}_i, \epsilon)} d\mathbf{z}} \leq 1 \quad (29)$$

Because $p_\theta(\mathbf{z}) = N(\boldsymbol{\mu}, \boldsymbol{\Sigma})$, it is reasonable to assume that its conditional distribution is also a normal distribution, then:

$$p_\theta(\mathbf{z}|y=c) = N(\boldsymbol{\mu}_c, \boldsymbol{\Sigma}_c) \quad (30)$$

where $\boldsymbol{\mu}_{\Sigma_c} \in \mathbb{R}^d$; $\boldsymbol{\Sigma}_c \in \mathbb{R}^{d \times d}$ Moreover, because $p_\theta(\mathbf{z}|y=c)$ is dependent on label c , then it is reasonable to have the following :

$$\sum_{\mathbf{z}_i \in \mathcal{D}_{\hat{y}=c}^z} (\mathbf{z}_i - \boldsymbol{\mu}_c)^\top (\mathbf{z}_i - \boldsymbol{\mu}_c) \leq \sum_{\mathbf{z}_i \in \mathcal{D}_{y=c}^z} (\mathbf{z}_i - \boldsymbol{\mu})^\top (\mathbf{z}_i - \boldsymbol{\mu}) \quad (31)$$

where $\forall \mathbf{z}_i \int_{\theta_D}(\mathbf{z}_i) \in y_c$. Intuitively, 31 means that the latent code of each training sample conditioned on the label $y=c$ is more centered around the learned latent space of distribution $p_\theta(\mathbf{z}|y=c)$ than centered around the learned space of distribution $p_\theta(\mathbf{z})$.

Then, we look into the KL divergence $\int p_\theta(\mathbf{z}|y=c) \log \frac{p_\theta(\mathbf{z}|y=c)}{q(\mathbf{z}; \mathbf{z}_i)} d\mathbf{z}$

$$\int p_\theta(\mathbf{z}|y=c) \log \frac{p_\theta(\mathbf{z}|y=c)}{q(\mathbf{z}; \mathbf{z}_i)} d\mathbf{z} \quad (32)$$

$$= \int p_\theta(\mathbf{z}|y=c) \log p_\theta(\mathbf{z}|y=c) d\mathbf{z} - \int p_\theta(\mathbf{z}|y=c) \log q(\mathbf{z}; \mathbf{z}_i) d\mathbf{z} \quad (33)$$

$$= -\frac{d}{2} (1 + \log 2\pi) - \frac{1}{2} \log \det(\boldsymbol{\Sigma}_c) + \mathbb{E}_{\mathbf{z} \sim p_\theta(\mathbf{z}|y=c)} (-\log q(\mathbf{z}; \mathbf{z}_i)) \quad (34)$$

$$= \frac{1}{2} \left[\frac{(\mathbf{z}_i - \boldsymbol{\mu}_c)^\top (\mathbf{z}_i - \boldsymbol{\mu}_c)}{\epsilon} - \log \frac{\det(\boldsymbol{\Sigma}_c)}{\epsilon^d} + \frac{\text{Tr}(\boldsymbol{\Sigma}_c)}{\epsilon} - d \right] \quad (35)$$

We use the SVD decomposition to decompose the $\boldsymbol{\Sigma}$:

$$\boldsymbol{\Sigma}_c = U_c \Lambda_c U_c^\top \quad (36)$$

And:

$$\log \det \boldsymbol{\Sigma}_c = \log \det U_c \Lambda_c U_c^\top = \log |U_c| | \Lambda_c | |U_c^\top| = \log | \Lambda_c | \quad (37)$$

$$\text{Tr}(\boldsymbol{\Sigma}_c) = \text{Tr}(U_c \Lambda_c U_c^\top) = \text{Tr}(\Lambda_c U_c U_c^\top) = \text{Tr}(\Lambda_c) \quad (38)$$

Then 35 equals to the following:

$$\frac{1}{2} \left[\frac{(\mathbf{z}_i - \boldsymbol{\mu}_c)^\top (\mathbf{z}_i - \boldsymbol{\mu}_c)}{\epsilon} - \log \frac{\det(\Lambda_c)}{\epsilon^d} + \frac{\text{Tr}(\Lambda_c)}{\epsilon} - d \right] \quad (39)$$

Similarly:

$$\int p_\theta(\mathbf{z}) \log \frac{p_\theta(\mathbf{z})}{q(\mathbf{z}; \mathbf{z}_i)} d\mathbf{z} \quad (40)$$

$$= \frac{1}{2} \left[\frac{(\mathbf{z}_i - \boldsymbol{\mu})^\top (\mathbf{z}_i - \boldsymbol{\mu})}{\epsilon} - \log \frac{\det(\boldsymbol{\Sigma}_c)}{\epsilon^d} + \frac{\text{Tr}(\boldsymbol{\Sigma}_c)}{\epsilon} - d \right] \quad (41)$$

$$= \frac{1}{2} \left[\frac{(\mathbf{z}_i - \boldsymbol{\mu})^\top (\mathbf{z}_i - \boldsymbol{\mu})}{\epsilon} - \log \frac{\det(\Lambda)}{\epsilon^d} + \frac{\text{Tr}(\Lambda)}{\epsilon} - d \right] \quad (42)$$

where

$$\Sigma = U \Lambda U^T \quad (43)$$

According to the assumption, the nuclear norm of the two covariance matrices is different, to be specific:

$$\|\Sigma_c\|_* \leq \|\Sigma\|_* \quad (44)$$

Namely, according to the definition of the nuclear norm, we have:

$$\text{Tr}(\Lambda_c) \leq \text{Tr}(\Lambda) \quad (45)$$

Then

$$\lim_{\epsilon \rightarrow 0} \frac{\sum_{\mathbf{z}_i \in \mathcal{D}_{y=c}^z} \int p_\theta(\mathbf{z}|y=c) \log \frac{p_\theta(\mathbf{z}|y=c)}{q(\mathbf{z}, \mathbf{z}_i, \epsilon)} d\mathbf{z}}{\sum_{\mathbf{z}_i \in \mathcal{D}_{y=c}^z} \int p_\theta(\mathbf{z}) \log \frac{p_\theta(\mathbf{z})}{q(\mathbf{z}, \mathbf{z}_i, \epsilon)} d\mathbf{z}} \quad (46)$$

$$\Rightarrow \lim_{\epsilon \rightarrow 0} \frac{\left[\frac{(\mathbf{z}_i - \boldsymbol{\mu}_c)^\top (\mathbf{z}_i - \boldsymbol{\mu}_c)}{\epsilon} - \log \frac{\det(\Lambda_c)}{\epsilon^d} + \frac{\text{Tr}(\Lambda_c)}{\epsilon} - d \right]}{\left[\frac{(\mathbf{z}_i - \boldsymbol{\mu})^\top (\mathbf{z}_i - \boldsymbol{\mu})}{\epsilon} - \log \frac{\det(\Lambda)}{\epsilon^d} + \frac{\text{Tr}(\Lambda)}{\epsilon} - d \right]} \quad (47)$$

$$(48)$$

Then we use the L'Hospital's rule:

$$\lim_{\epsilon \rightarrow 0} \frac{\left[-1 \frac{(\mathbf{z}_i - \boldsymbol{\mu}_c)^\top (\mathbf{z}_i - \boldsymbol{\mu}_c)}{\epsilon^2} + \frac{d}{\epsilon} - \frac{\text{Tr}(\Lambda_c)}{\epsilon^2} \right]}{\left[-1 \frac{(\mathbf{z}_i - \boldsymbol{\mu})^\top (\mathbf{z}_i - \boldsymbol{\mu})}{\epsilon^2} + \frac{d}{\epsilon} - \frac{\text{Tr}(\Lambda)}{\epsilon^2} \right]} \quad (49)$$

$$= \frac{(\mathbf{z}_i - \boldsymbol{\mu}_c)^\top (\mathbf{z}_i - \boldsymbol{\mu}_c) + \text{Tr}(\Lambda_c)}{(\mathbf{z}_i - \boldsymbol{\mu})^\top (\mathbf{z}_i - \boldsymbol{\mu}) + \text{Tr}(\Lambda)} \quad (50)$$

$$\leq 1 \quad (51)$$

B

The expectation of N_{mem} is easy to get by using the definition of the expectation: $\mathbb{E}(N_{\text{mem}})$

$$\mathbb{E}(N_{\text{mem}}) = \sum_{i=1}^M N_G p_\gamma(x_i) = N_G \sum_{i=1}^M p_\gamma(x_i) \quad (52)$$

To prove the expectation $\mathbb{E}(N_{\text{umem}})$, we firstly define a new variable I_i . It means the image i is generated in the N_G -th generation, the probability of it is:

$$p(I_i) = 1 - (1 - p_\gamma(i))^{N_G} \quad (53)$$

Then, according to the linear property of expectation, it is easy to get:

$$\mathbb{E}(N_{\text{umem}}) \quad (54)$$

$$= \mathbb{E}(I_1) + \mathbb{E}(I_2) + \cdots + \mathbb{E}(I_M) \quad (55)$$

$$= \sum_{i=1}^M 1 - (1 - p_\gamma(i))^{N_G} \quad (56)$$

C

The integration of the time module directly after batch normalization within the network architecture is a reasonable design choice rooted in the functionality of batch normalization itself. Batch normalization standardizes the inputs to the network layer, stabilizing the learning process by reducing

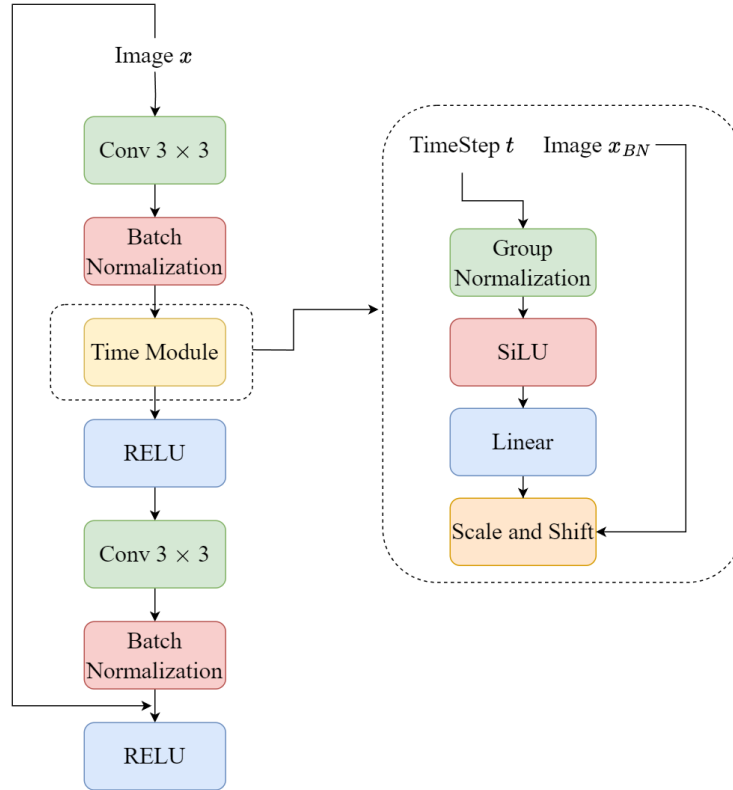


Figure 6: Refinement ResNet block with time-dependent module integration. This block diagram depicts the insertion of a time module within a conventional ResNet block architecture, allowing the network to respond to the data’s timesteps. Image x_{BN} is the image processed after the first Batch Normalization Layer.

internal covariate shifts. By positioning the time module immediately after this normalization process, the model can introduce time-dependent adaptations to the already stabilized features. This placement ensures that the temporal adjustments are applied to a normalized feature space, thereby enhancing the model’s ability to learn temporal dynamics effectively.

Moreover, the inclusion of the time module at a singular point within the network strikes a balance between model complexity and temporal adaptability. This singular addition avoids the potential redundancy and computational overhead that might arise from multiple time modules. It allows the network to maintain a streamlined architecture while still gaining the necessary capacity to handle time-varying inputs.

D

Table 2: Generate Training Epoch: 3000 Dataset: CelebA-HQ-FI Generate Num Per λ : 50000. The AMS and UMS is measured on Mid Similarity

| λ | AMS(%) | UMS(%) | Top 0.1% | Top 0.5% | Top 1.0% | Top 5.0% | Top 10.0% |
|-----------|--------------|--------------|--------------|--------------|--------------|--------------|--------------|
| 0 | 0.596 | 0.328 | 0.604 | 0.544 | 0.518 | 0.463 | 0.440 |
| 1 | 0.588 | 0.312 | 0.596 | 0.540 | 0.517 | 0.463 | 0.440 |
| 2 | 0.640 | 0.350 | 0.591 | 0.541 | 0.518 | 0.465 | 0.441 |
| 3 | 0.764 | 0.386 | 0.594 | 0.549 | 0.525 | 0.470 | 0.446 |
| 4 | 0.850 | 0.390 | 0.604 | 0.553 | 0.529 | 0.473 | 0.448 |
| 5 | 0.952 | 0.436 | 0.596 | 0.551 | 0.530 | 0.476 | 0.451 |
| 6 | 1.092 | 0.414 | 0.611 | 0.560 | 0.536 | 0.480 | 0.454 |
| 7 | 1.110 | 0.446 | 0.607 | 0.562 | 0.539 | 0.482 | 0.457 |
| 8 | 1.148 | 0.444 | 0.618 | 0.566 | 0.542 | 0.484 | 0.458 |
| 9 | 1.274 | 0.478 | 0.615 | 0.567 | 0.544 | 0.485 | 0.459 |
| 10 | 1.338 | 0.444 | 0.613 | 0.569 | 0.546 | 0.487 | 0.461 |
| 11 | 1.292 | 0.454 | 0.604 | 0.562 | 0.541 | 0.486 | 0.460 |
| 12 | 1.262 | 0.406 | 0.617 | 0.567 | 0.544 | 0.486 | 0.460 |
| 13 | 1.390 | 0.432 | 0.617 | 0.569 | 0.546 | 0.489 | 0.462 |
| 14 | 1.232 | 0.384 | 0.613 | 0.567 | 0.544 | 0.485 | 0.459 |
| 15 | 1.516 | 0.462 | 0.616 | 0.570 | 0.548 | 0.490 | 0.463 |
| 16 | 1.280 | 0.390 | 0.612 | 0.566 | 0.543 | 0.487 | 0.461 |
| 17 | 1.282 | 0.386 | 0.605 | 0.561 | 0.541 | 0.486 | 0.460 |
| 18 | 1.330 | 0.374 | 0.616 | 0.569 | 0.545 | 0.488 | 0.461 |
| 19 | 1.204 | 0.354 | 0.612 | 0.564 | 0.541 | 0.485 | 0.460 |
| 20 | 1.178 | 0.358 | 0.603 | 0.559 | 0.538 | 0.483 | 0.458 |
| 21 | 1.172 | 0.342 | 0.617 | 0.566 | 0.542 | 0.484 | 0.459 |
| 22 | 1.208 | 0.368 | 0.602 | 0.560 | 0.539 | 0.485 | 0.459 |
| 23 | 1.286 | 0.302 | 0.607 | 0.561 | 0.540 | 0.485 | 0.459 |
| 24 | 1.244 | 0.352 | 0.597 | 0.558 | 0.538 | 0.484 | 0.458 |
| 25 | 1.198 | 0.340 | 0.599 | 0.560 | 0.538 | 0.483 | 0.458 |
| 26 | 1.220 | 0.338 | 0.601 | 0.559 | 0.539 | 0.483 | 0.458 |
| 27 | 1.128 | 0.320 | 0.608 | 0.561 | 0.538 | 0.483 | 0.457 |
| 28 | 1.102 | 0.314 | 0.604 | 0.556 | 0.534 | 0.481 | 0.456 |
| 29 | 1.034 | 0.290 | 0.595 | 0.556 | 0.534 | 0.481 | 0.456 |
| 30 | 1.026 | 0.326 | 0.602 | 0.557 | 0.535 | 0.480 | 0.455 |
| 31 | 1.020 | 0.268 | 0.591 | 0.551 | 0.531 | 0.479 | 0.455 |
| 32 | 1.054 | 0.282 | 0.593 | 0.551 | 0.531 | 0.479 | 0.455 |
| 33 | 1.106 | 0.306 | 0.600 | 0.555 | 0.535 | 0.481 | 0.456 |
| 34 | 1.062 | 0.288 | 0.582 | 0.547 | 0.529 | 0.479 | 0.454 |
| 35 | 0.922 | 0.266 | 0.587 | 0.547 | 0.527 | 0.477 | 0.453 |
| 36 | 0.874 | 0.260 | 0.585 | 0.545 | 0.525 | 0.477 | 0.453 |
| 37 | 0.964 | 0.258 | 0.589 | 0.549 | 0.528 | 0.477 | 0.452 |
| 38 | 0.888 | 0.246 | 0.582 | 0.543 | 0.524 | 0.475 | 0.452 |
| 39 | 0.940 | 0.274 | 0.587 | 0.548 | 0.528 | 0.476 | 0.452 |
| 40 | 0.808 | 0.234 | 0.587 | 0.544 | 0.524 | 0.474 | 0.451 |
| 41 | 0.870 | 0.252 | 0.582 | 0.543 | 0.524 | 0.476 | 0.452 |
| 42 | 0.872 | 0.238 | 0.584 | 0.543 | 0.523 | 0.475 | 0.451 |
| 43 | 0.856 | 0.244 | 0.584 | 0.545 | 0.525 | 0.475 | 0.451 |
| 44 | 0.796 | 0.212 | 0.578 | 0.540 | 0.521 | 0.473 | 0.449 |
| 45 | 0.770 | 0.242 | 0.580 | 0.538 | 0.519 | 0.472 | 0.449 |
| 46 | 0.774 | 0.218 | 0.580 | 0.540 | 0.521 | 0.472 | 0.448 |
| 47 | 0.754 | 0.214 | 0.581 | 0.542 | 0.521 | 0.471 | 0.448 |
| 48 | 0.716 | 0.218 | 0.572 | 0.536 | 0.518 | 0.471 | 0.448 |
| 49 | 0.694 | 0.216 | 0.570 | 0.533 | 0.515 | 0.469 | 0.446 |
| 50 | 0.728 | 0.204 | 0.576 | 0.535 | 0.518 | 0.471 | 0.447 |